Asymmetric Squares as an Attracting Set in Rayleigh-Bénard Convection

F. H. Busse and R. M. Clever

Institute of Physics, University of Bayreuth, D-95440 Bayreuth, Germany
and Institute of Physics and Planetary Physics, UCLA, Los Angeles, California 90024

(Received 19 December 1997)

Properties of asymmetric square convection in a horizontal fluid layer heated from below are studied numerically with a Galerkin method. Since the Boussinesq approximation is used and symmetric rigid boundaries are assumed, both types of asymmetric square convection—those with rising and those with descending motion in the center—are physically equivalent. It is shown that asymmetric square convection becomes stable with respect to arbitrary three-dimensional infinitesimal disturbances for Rayleigh numbers in excess of 3 to 4 times the critical value. [S0031-9007(98)06556-9]

PACS numbers: 47.20.Ky, 47.27.–i

In the investigation of attracting manifolds of solutions describing convection in fluid layers heated from below the attention has been focused on two-dimensional rolls and solutions bifurcating from that manifold. It is well known that rolls represent the only stable form of convection at Rayleigh numbers R close to the critical value R_c when the Boussinesq approximation can be assumed [1]. But at higher values of the control parameter R other manifolds of stable solutions exist which may not be connected through bifurcations to the manifold of rolls. An example of such a manifold of solutions is convection flows with hexagonal symmetry in their two manifestations with either up- or downgoing motions in the center of the hexagonal cell. Assenheimer and Steinberg [2] have realized both types of hexagonal convection in a Rayleigh-Bénard experiment at values of R in excess of twice the critical value. Through a stability analysis [3] it has later been established that these dual types of hexagonal convection do indeed become stable in regions of the Rayleigh-wave number space where they have been observed in the experiment. Because the Boussinesq approximation was employed in the theoretical analysis the results of the latter clearly demonstrate that the cause for the realization of the dual type of hexagons is quite different from the non-Boussinesq effects that lead to a preference for either up or down hexagons near the critical value of R.

In this paper we intend to demonstrate that a similar property holds for convection flows in the form of asymmetric squares. Asymmetric squares differ from the dual hexagons essentially only in that the hexagonal boundary is replaced by a square boundary. Like hexagonal cells asymmetric square convection cells, usually with rising motion in the center, are observed in convection layers with strong asymmetries with respect to the midplane as, for instance, in the case of fluids with strongly temperature dependent viscosity [4] or in the case of Marangoni convection [5]. For corresponding theoretical work see [6] and [7]. By contrast the analysis of the present paper focuses on the unexpected occurrence of asymmetric squares in layers with symmetry about the midplane.

Like the dual hexagons in a symmetric convection layer the asymmetric squares appear in two physically equivalent forms which differ by the sign of the vertical motion in the center of the cells. In the following we shall first derive the basic equations and describe the method of the numerical analysis. We then proceed to the presentation of the results for selected Prandtl numbers.

We consider a horizontal fluid layer of depth h with the temperatures T_1 and T_2 fixed at the upper and lower rigid boundaries. Using the length scale h, the time scale h^2/κ where κ is the thermal diffusivity, and the temperature scale $T_2 - T_1$, we write the Boussinesq equations of motion for the velocity vector $\vec{u}$ and the heat equation for the deviation θ of the temperature from its static distribution in the dimensionless form

$$P^{-1}\left(\frac{\partial}{\partial t}\vec{u} + \vec{u}\cdot\nabla\vec{u}\right) = -\nabla\pi + \vec{\lambda}\theta R + \nabla^2\vec{u}\,, \quad \text{(1a)}$$

$$\nabla\cdot\vec{u} = 0\,, \quad \text{(1b)}$$

$$\frac{\partial}{\partial t}\theta + \vec{u}\cdot\nabla\theta = \vec{\lambda}\cdot\vec{u} + \nabla^2\theta\,, \quad \text{(1c)}$$

where $\vec{\lambda}$ is the vertical unit vector opposite to the direction of gravity, π is the deviation of the pressure from its static value, and where the Rayleigh number R and the Prandtl number P are defined by

$$R = \frac{\gamma(T_2 - T_1)gh^3}{\nu\kappa}, \qquad P = \frac{\nu}{\kappa}\,. \quad \text{(2)}$$

g, γ, and ν denote the acceleration of gravity, the coefficient of thermal expansion, and the kinematic viscosity, respectively. In order to eliminate Eq. (1b) we introduce the following general representation for solenoidal vector fields in the absence of mean flows:

$$\vec{u} = \nabla\times(\nabla\times\vec{\lambda}\varphi) + \nabla\times\vec{\lambda}\psi\,. \quad \text{(3)}$$

Steady three-dimensional solutions of Eqs. (1) can be obtained through the Galerkin ansatz,

$$\varphi = \sum_{l,m,n} a_{lmn}\cos(l\alpha x)\cos(m\alpha y)f_n(z)\,, \quad \text{(4a)}$$

$$\psi = \sum_{l,m,n} c_{lmn} \sin(l\alpha x) \sin(m\alpha y) \sin n\pi(z + \tfrac{1}{2}), \quad (4b)$$

$$\theta = \sum_{l,m,n} b_{lmn} \cos(l\alpha x) \cos(m\alpha y) \sin n\pi(z + \tfrac{1}{2}), \quad (4c)$$

where a Cartesian system of coordinates has been introduced with the z coordinate in the vertical direction and where $f_n(z)$ denotes the Chandrasekhar functions [8] which obey the conditions $f_n = df_n/dz = 0$ at $z = \pm\frac{1}{2}$. The boundary conditions

$$\varphi = \partial\varphi/\partial z = \psi = \theta = 0 \quad \text{for } z = \pm\tfrac{1}{2} \quad (5)$$

at the rigid, isothermal boundaries are thus satisfied by the representations (4). Since the functions $f_n(z)$ form a complete set like the trigonometric functions, general z dependences satisfying the conditions (5) can be described by the representations (4).

Once the z components of the curlcurl and of the curl of Eqs. (1a) and (1c) have been projected onto the sets of expansion functions introduced in expressions (4), a system of nonlinear algebraic equations for the unknowns $a_{lmn}, b_{lmn}, c_{lmn}$ is obtained. This system can be solved through a Newton-Raphson method after a truncation has been introduced. We shall disregard all coefficients and corresponding equations satisfying

$$l + m + n > N_T, \quad (6)$$

where N_T is chosen sufficiently high in order that sensitive integral properties such as the convective heat transfer do not change by more than 1% when N_T is replaced by $N_T - 2$. Typically values between 10 and 14 have been used for N_T, depending on the Rayleigh number.

Among the solutions described by the representation (4) those with a square symmetry are characterized by the property that the coefficients are symmetric in the subscripts l and m. A subset of these solutions with the property

$$a_{lnm} = b_{lmn} = 0 \quad \text{for } l + m + n = \text{ odd}, \qquad c_{lmn} = 0 \quad \text{for } l + m + n = \text{ even} \quad (7)$$

describe symmetric square convection. With $\alpha = \alpha_c$, this kind of solution exists at the critical value R_c of R, but it is unstable [1], and it is generally believed that it remains unstable at higher values of R except at very high values of R and P [9]. Convection in the form of asymmetric squares exists as up squares or as down squares, corresponding to opposite signs of the coefficients a_{lmn} with odd $l + m + n$, while those with even $l + m + n$ have the same values,

$$a^{(u)}_{lmn} = (-1)^{l+m+n} a^{(d)}_{lmn}, \qquad b^{(u)}_{lmn} = (-1)^{l+m+n} b^{(d)}_{lmn}, \qquad c^{(u)}_{lmn} = -(-1)^{l+m+n} c^{(d)}_{lmn}. \quad (8)$$

An example of steady down-square convection is shown in Fig. 1, which also serves to illustrate up-square convection after an appropriate transformation. The dependence of the Nusselt number and kinetic energies of asymmetric square convection on the Rayleigh number are shown in Fig. 2. It is of interest to see that the Nusselt number exceeds that of two-dimensional rolls with the same wave number α. As in the case of hexagonal convection we attribute this effect to stronger contributions of higher harmonics in asymmetric square convection.

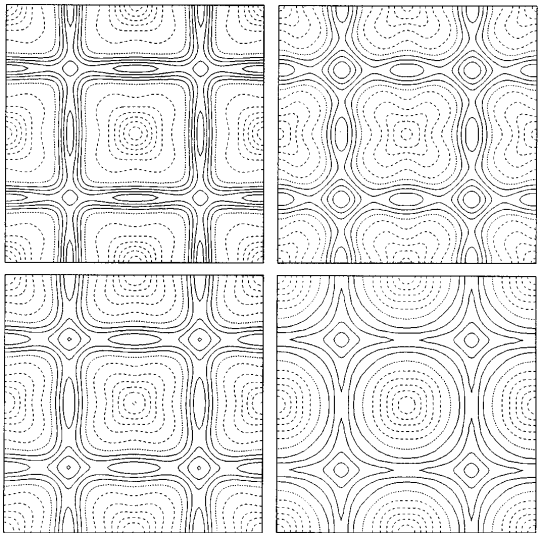

FIG. 1. Lines of constant vertical velocity in the planes $z = -0.4$ (upper left), $z = 0.4$ (upper right), $z = 0$ (lower left), and isotherms in the plane $z = 0$ (lower right) in the case of asymmetric down-square convection for $R = 10^4, P = 7, \alpha = 2.0$. Solid (dashed) lines indicate positive (negative) values. The plots also describe asymmetric up-square convection when the planes $z = \pm 0.4$ are interchanged and dashed (solid) lines are interpreted as positive (negative) values.

In order to study the stability of asymmetric square convection we superimpose onto the steady solutions of the form (4) infinitesimal disturbances of the general form

$$\tilde{\varphi} = \exp\{idx + iby + \sigma t\} \times \sum_{l,m,n} \tilde{a}_{lmn} \exp\{il\alpha x + im\alpha y\} f_n(z), \quad (9)$$

with analogous expressions for $\tilde{\psi}, \tilde{\theta}$. After projection of the linearized equations for $\tilde{\varphi}, \tilde{\theta}$, and $\tilde{\psi}$ onto the expansion functions, a system of linear homogeneous equations for the coefficients $\tilde{a}_{lmn}, \tilde{b}_{lmn}, \tilde{c}_{lmn}$ is obtained with the growth rate σ as eigenvalue. For a given steady asymmetric square solution characterized by the parameters R, P, and α the eigenvalue σ with maximum real part σ_r is determined as a function of the Floquet wave numbers b and d. Whenever an eigenvalue exists with positive σ_r the steady solution is unstable, otherwise it is stable with respect to infinitesimal disturbances.

Results for stability of asymmetric square convection are shown as a function of R and α in the case $P = 7$ in Fig. 3. Two kinds of stability boundaries in the R-α plane are displayed. The outer stability boundaries

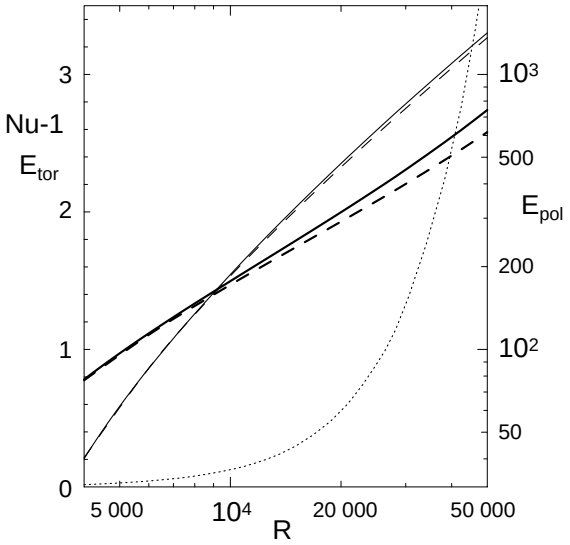

FIG. 2. Nusselt number (thick solid line) and kinetic energies of the poloidal (thin solid line, left ordinate) and of the toroidal (dotted line, left ordinate) components of motion corresponding to the first and second terms in the representation (3), respectively, for asymmetric square convection in the case $P = 7, \alpha = 2.2$. Also shown by dashed lines are the corresponding values for two-dimensional rolls.

correspond to disturbances with $d = b = 0$, i.e., they do not tend to change the periodicity interval of the steady solution. These stability boundaries could be of physical interest in the case of a small aspect ratio layer where only a few square cells are realized. For an extended layer, however, the general stability analysis with no restriction on the wave numbers b and d is relevant. Figure 3 demonstrates the fact that there exists a region of Rayleigh numbers extending from above 6×10^3 to about 27×10^3 where steady asymmetric square convection is stable with respect to general infinitesimal disturbances. The wave number of the stable square cells is considerably smaller than the critical value α_c and tends to decrease with increasing Rayleigh number. Problems of numerical convergence for solutions with $\alpha = 1.2$ have prevented us from determining the stability boundary towards low values of α. It is of interest to note that the most strongly growing disturbances outside the stability region are subharmonic disturbances. Towards lower values of R, the strongest growing disturbances are usually subharmonic in one dimension, i.e., they correspond to $d = \alpha/2, b = 0$ or $b = \alpha/2, d = 0$ for reasons of symmetry. Towards higher values of R doubly subharmonic disturbances with $d = b = \alpha/2$ are the most critical ones. The boundary towards high wave numbers corresponds to disturbances with $b = d = 0$. These disturbances tend to provide the transition to rolls in one of the two directions defined by the squares.

Results analogous to those found in the case $P = 7$ are obtained when the Prandtl number is increased to 16

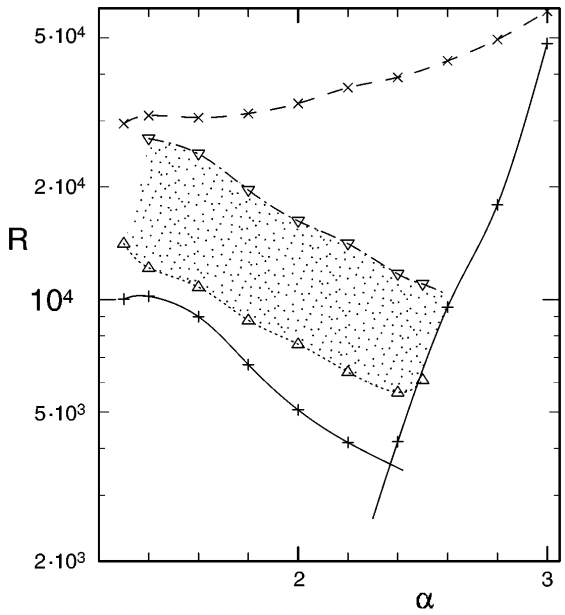

FIG. 3. The region of stable asymmetric squares (shaded) in the R-α space for $P = 7$ is bounded by the singly subharmonic instability ($\triangle$) from below and by the doubly subharmonic instability ($\triangledown$) from above. The boundary towards high α indicates the transition to rolls. Also shown are the boundaries (denoted by $\times$ or $+$) beyond which disturbances are growing that do not change the horizontal periodicity of asymmetric square convection.

as shown in Fig. 4. Again a range of stable asymmetric square convection exists for Rayleigh numbers above 6×10^3. When the Prandtl number is decreased to 2.5 a range of stable asymmetric square convection can be obtained only when disturbances are restricted to those with

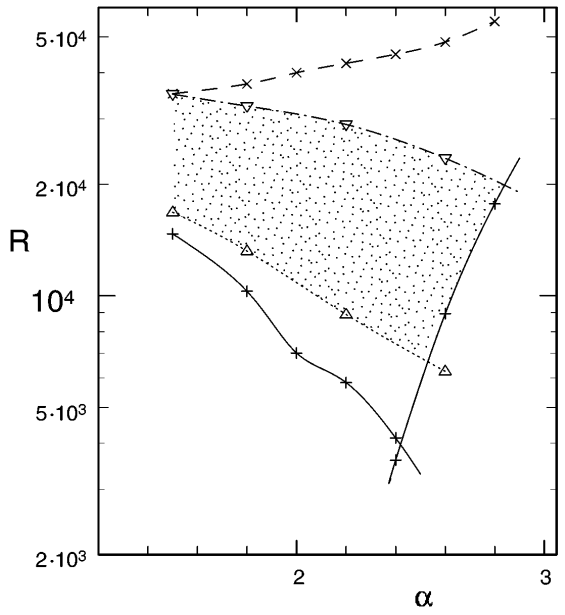

FIG. 4. Same as Fig. 3, but in the case $P = 16$.

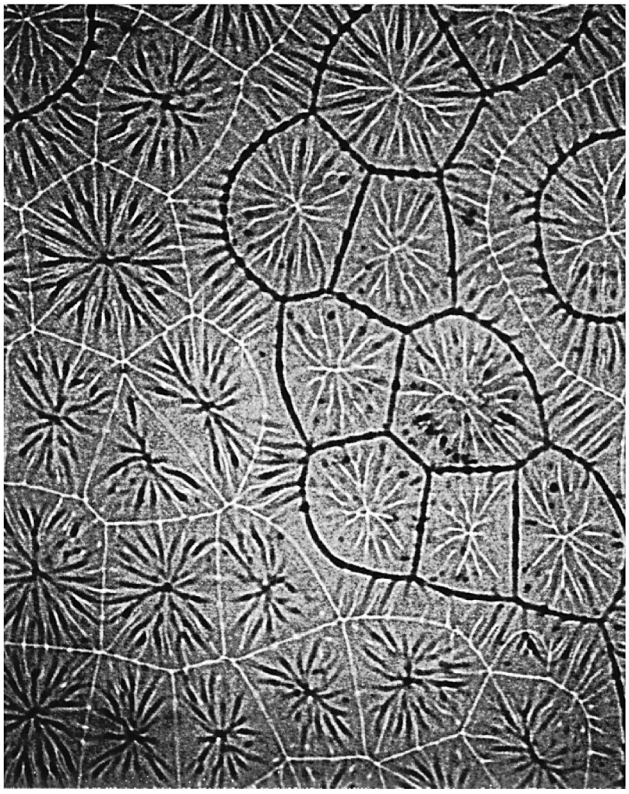

FIG. 5. Convection pattern in a layer of methyl alcohol ($P = 7$) at about 23 °C with $h = 5.6$ mm heated from below made visible by a shadowgraph method (for details see [10]) at a Rayleigh number of about 45 000. Dark (white) lines indicate rising (descending) motions.

$d = b = 0$. With respect to the latter-type disturbances the stability boundaries resemble the corresponding ones in Figs. 3 and 4. Without the restriction $b = d = 0$ growing disturbances are found for $P = 2.5$ in all parts of the relevant domain in the R-α plane.

Our theoretical results indicate that asymmetric square convection should be observable in laboratory experiments. Controlled initial conditions may have to be used to reach the region of stable asymmetric squares in the parameter space. An experimental observation indicating a tendency towards asymmetric square cells—as well as hexagonal cells—is shown in Fig. 5. This photograph of a shadowgraph image of convection in methyl alcohol was taken in connection with experiments described in [10]. Since cells with rising motion in the center and those with descending motion have the same stability properties, it is unlikely that a periodic pattern will be found in experiments with extended symmetric convection layers unless controlled initial conditions are used. Instead domains with either types of cells are expected to be realized as has been demonstrated in [2] or can be seen in Fig. 5. The observation of Fig. 5 was made after the convection layer had been left at a constant value of $R = 45 \times 10^3$ for 12 hours. Because this value is higher than those studied theoretically and because the convection motion in the interior of the cells is not steady in the experiment, the observations cannot be compared directly with the theory. They just serve as a reminder that several kinds of attractors compete in realizations of Rayleigh-Bénard convection at elevated Rayleigh numbers and domains of these attractors separated by roll-like boundaries appear to be a typical feature of extended convection layers.

[1] A. Schlüter, D. Lortz, and F. Busse, J. Fluid Mech. **23**, 129–144 (1965).
[2] M. Assenheimer and V. Steinberg, Phys. Rev. Lett. **76**, 756–759 (1996).
[3] R. M. Clever and F. H. Busse, Phys. Rev. E **53**, R2037–R2040 (1996).
[4] D. S. Oliver and J. R. Booker, Geophys. Astrophys. Fluid Dyn. **27**, 73–85 (1983).
[5] K. Nitschke and A. Thess, Phys. Rev. E **52**, R5772–R5775 (1995).
[6] F. H. Busse and H. Frick, J. Fluid Mech. **150**, 451–465 (1985).
[7] M. Bestehorn, Phys. Rev. Lett. **76**, 46–49 (1996).
[8] S. Chandrasekhar, *Hydrodynamic and Hydromagnetic Stability* (Clarendon, Oxford, 1961).
[9] J. A. Whitehead and B. Parsons, Geophys. Astrophys. Fluid Dyn. **9**, 201–217 (1978).
[10] F. H. Busse and R. M. Clever, J. Fluid Mech. **91**, 319–335 (1979).